of the NH---S hydrogen bonds in **4–7** in a weakly nonpolar solvent such as DME is in the order X = OMe < H < F < CN. The electron density on the S atom of the peptide ligand was decreased by the electron-withdrawing substituent through the NH---S hydrogen bond and gave a positive shift of the redox potentials.[6]

Conclusion

Form this study, the NH---S hydrogen bonds were found to play an important role in controlling the redox potentials. The observed positively shifted redox potential in native Rd is thus also interpreted by the formation of the same types of NH---S hydrogen bonds. The observation of the charge flow through the NH---S hydrogen bond makes it possible that the hydrogen bond is one of the candidates for a channel for electron transfer in Rd.

Our model complexes exhibited an absorption maximum around 330 nm similar to that in native Rd. It has been thought that there is some kind of electronic interaction between the coordinated sulfur atom and the phenyl rings.[23,24] Further study is required in order to assign the absorption maximum and to understand the effect of the phenyl rings of tyrosyl and phenylalanyl residues close to the Fe ion in Rd.

Registry No. Z-Cys(Acm)-Pro-Leu-OH, 82154-63-0; HCl·Cys(Acm)-Gly-NH-C_6H_5, 135615-70-2; Z-Cys(Acm)-Pro-Leu-Cys(Acm)-Gly-NH-C_6H_5, 135615-71-3; Z-Cys(Acm)-Pro-Leu-Cys(Acm)-Gly-NH-C_6H_4-*p*-OMe, 135615-72-4; Z-Cys(Acm)-Pro-Leu-Cys(Acm)-Gly-NH-C_6H_4-*p*-F, 135615-73-5; Z-Cys(Acm)-Pro-Leu-Cys(Acm)-Gly-NH-C_6H_4-*p*-CN, 135615-74-6; Z-Cys(Acm)-Pro-Leu-Cys(Acm)-Gly-NH-C_6H_4-*m*-F, 135615-75-7; Z-Cys(SH)-Pro-Leu-Cys(SH)-Gly-NH-C_6H_4-*p*-OMe, 135615-77-9; Z-Cys(SH)-Pro-Leu-Cys(SH)-Gly-NH-C_6H_5, 135615-78-0; Z-Cys(SH)-Pro-Leu-Cys(SH)-Gly-NH-C_6H_4-*p*-F, 135615-76-8; Z-Cys(SH)-Pro-Leu-Cys(SH)-Gly-NH-C_6H_4-*p*-CN, 135615-79-1; $(Et_4N)_2$[Fe(Z-Cys-Pro-Leu-Cys-Gly-NH-C_6H_4-*p*-OMe)$_2$], 135619-95-3; $(Et_4N)_2$[Fe(Z-Cys-Pro-Leu-Cys-Gly-NH-C_6H_5)$_2$], 135619-97-5; $(Et_4N)_2$[Fe(Z-Cys-Pro-Leu-Cys-NH-C_6H_4-*p*-F)$_2$], 135619-99-7; $(Et_4N)_2$[Fe(Z-Cys-Pro-Leu-Cys-Gly-NH-C_6H_4-*p*-CN)$_2$], 135620-01-8; Z-Cys(SH)-Pro-Leu-Cys(SH)-Gly-NH-C_6H_4-*m*-F, 135615-80-4; $(Et_4N)_2$[Fe(Z-Cys-Pro-Leu-Cys-Gly-NH-C_6H_4-*m*-F)$_2$], 135638-53-8; Z-Cys(SH)-Pro-Leu-Cys(SH)-Gly-N^{2}H-C_6H_4-*p*-OMe, 135615-81-5; Z-Cys(SH)-Pro-Leu-Cys(SH)-Gly-N^{2}H-C_6H_5, 135615-82-6; Z-Cys(SH)-Pro-Leu-Cys(SH)-Gly-N^{2}H-C_6H_4-*p*-F, 135615-83-7; Z-Cys(SH)-Pro-Leu-Cys(SH)-Gly-N^{2}H-C_6H_4-*p*-CN, 135615-84-8; $[Fe^{II}$(Z-Cys-Pro-Leu-Cys-Gly-NH-C_6H_4-*p*-OMe)$_2]^{2-}$, 135619-94-2; $[Fe^{II}$(Z-Cys-Pro-Leu-Cys-Gly-NH-C_6H_5)$_2]^{2-}$, 135619-96-4; $[Fe^{II}$(Z-Cys-Pro-Leu-Cys-Gly-NH-C_6H_4-*p*-F)$_2]^{2-}$, 135619-98-6; $[Fe^{II}$-(Z-Cys-Pro-Leu-Cys-Gly-NH-C_6H_4-*p*-CN)$_2]^{2-}$, 135620-00-7.

(23) Frey, M.; Sieker, L.; Payan, F.; Haser, R.; Bruschi, M.; Pepe, G.; LeGall, J. *J. Mol. Biol.* **1987**, *197*, 525.
(24) Krishnamoorthi, R.; Markley, J. L.; Cusanovich, M. A.; Przysieki, C. T. *Biochemistry* **1986**, *25*, 50.

Contribution from the Department of Inorganic Chemistry, Indian Association for the Cultivation of Science, Calcutta 700 032, India

Mononuclear Manganese(IV) in Tridentate ONO Coordination. Synthesis, Structure, and Redox Regulation via Oxygen Donor Variation

Somnath Dutta, Partha Basu, and Animesh Chakravorty*

Received November 27, 1990

The aerobic reaction of *N*-(2-hydroxyphenyl)salicylaldimine (H_2amp) and 2,2′-dihydroxyazobenzene (H_2azp) with manganese(II) or manganese(III) affords $Mn^{IV}(amp)_2$ and $Mn^{IV}(azp)_2$, respectively. In a similar reaction, 2-hydroxy-2′-carboxy-5-methylazobenzene (H_2azc) furnishes $KMn^{III}(azc)_2 \cdot 4H_2O$, which can be oxidized to $Mn^{IV}(azc)_2$ by persulfate. The X-ray structures of $Mn(amp)_2$ and $Mn(azp)_2$ are reported. Crystal data for $Mn(amp)_2$: space group $C2/c$, $Z = 4$, $a = 20.163$ (12) Å, $b = 7.921$ (4) Å, $c = 12.994$ (10) Å, $\beta = 97.65$ (5)°, and $V = 2057$ (2) Å^3. Crystal data for $Mn(azp)_2$: space group $P\bar{1}$, $Z = 2$, $a = 7.766$ (5) Å, $b = 10.377$ (5) Å, $c = 12.964$ (5) Å, $\alpha = 92.80$ (3)°, $\beta = 90.33$ (5)°, $\gamma = 102.92$ (4)°, and $V = 1016.8$ (9) Å^3. The ligands act as meridional tridentate ONO donors. The Mn–O distances fall in the range 1.861 (4)–1.893 (6) Å. The Mn–N(azomethine) length, 1.968 (8) Å, is shorter than the average Mn–N(azo) length, 2.007 (10) Å. The MnO_4N_2 coordination spheres deviate considerably from octahedral geometry, and this is reflected in the EPR spectra of the complexes: strong and weak signals near $g = 4$ and $g = 2$, respectively. The manganese(IV)–manganese(III) reduction potentials of $Mn(amp)_2$, $Mn(azp)_2$, and $Mn(azc)_2$ in dimethyl sulfoxide are respectively −0.09, +0.15, and 0.31 V vs SCE. In MnO_4N_2-type salicylaldimine complexes, the potential varies with oxygen donors according to the order alcoholate < phenolate < carboxylate. The total shift can be as large as 600 mV. The trend is correlated with the p*K*'s of the oxygen donor functions. The significance of the results with respect to carboxylate binding of PS II manganese is noted.

Introduction

The coordination environment of the tetramanganese water oxidation site of photosystem II (PS II) consists of O and N donors,probably more of the former.[1-3] The metal oxidation state is generally believed to lie in the range 2+ to 4+. Plausible models of the tetrametal site span a number of alternatives.[2,4-9] Mononuclear manganese(IV) centers have been implicated[10] in the S_2 state of PS II. Synthetic monomanganese(IV) species in biomimetic O, N coordination are thus of interest. Authentic examples of such complexes are sparse, and structural characterization has been achieved in only a few cases.[11-19]

(1) Kirby, J. A.; Robertson, A. S.; Smith, J. P.; Thompson, A. C.; Cooper, S. R.; Klein, M. P. *J. Am. Chem. Soc.* **1981**, *103*, 5529–5537.
(2) (a) Guiles, R. D.; Zimmerman, J. L.; McDermott, A. E.; Yachandra, V.K.; Cole, J. L.; Dexheimer, S. L.; Britt, R. D.; Wieghardt, K.; Bossek, U.; Sauer, K.; Klein, M. P. *Biochemistry* **1990**, *29*, 471–485. (b) Yachandra, V. K.; Guiles, R. D.; McDermott, A. E.; Britt, R. D.; Dexheimer, S. L.; Sauer, K.; Klein, M. P. *Biochim. Biophys. Acta.* **1986**, *850*, 324–332.
(3) Tamura, N.; Ikeuchi, M.; Inoue, Y. *Biochim. Biophys. Acta.* **1989**, *973*, 281–289.
(4) George, G. N.; Prince, R. C.; Cramer, S. P. *Science* **1989**, *243*, 789–791.
(5) Yachandra, V. K.; Guiles, R. D.; McDermott, A. E.; Cole, J. E.; Britt, R. D.; Dexheimer, S. L.; Sauer, K.; Klein, M. P. *Biochemistry* **1987**, *26*, 5974–5981.
(6) Penner-Hahn, J. E.; Fronko, R. M.; Pecoraro, V. L.; Yocum, C. F.; Betts, S. D.; Bowlby, N. R. *J. Am. Chem. Soc.* **1990**, *112*, 2549–2557.
(7) Sivaraja, M.; Philo, J. S.; Lary, J.; Dismukes, G. C. *J. Am. Chem. Soc.* **1989**, *111*, 3221–3225.
(8) Brudvig, G. W.; Crabtree, R. H. *Proc. Natl. Acad. Sci. U.S.A.* **1986**, *83*, 4586–4588.
(9) Vincent, J. B.; Christou, G. *Adv. Inorg. Chem.* **1989**, *33*, 197–257.
(10) Hansoon, O.; Aasa, R.; Vangard, T. *Biophys. J.* **1987**, *51*, 825–832.
(11) Chandra, S. K.; Basu, P.; Ray, D.; Pal, S.; Chakravorty, A. *Inorg. Chem.* **1990**, *29*, 2423–2428.
(12) Chun, D. H.; Sawyer, D. T.; Schaeffer, W. P.; Simmons, C. J. *Inorg. Chem.* **1983**, *22*, 752–758.
(13) Lynch, M. W.; Hendrickson, D. N.; Fitzgerald, B. J.; Pierpont, C. G. *J. Am. Chem. Soc.* **1984**, *106*, 2041–2049.
(14) Hartman, J. R.; Foxman, B. M.; Cooper, S. R. *Inorg. Chem.* **1984**, *23*, 1381–1387.
(15) Kessissoglou, D. P.; Butler, W. M.; Pecoraro, V. L. *J. Chem. Soc., Chem. Commun.* **1986**, 1253–1255.
(16) Pavacik, P. S.; Huffman, J. C.; Christou, G. *J. Chem. Soc., Chem. Commun.* **1986**, 43–44.

0020-1669/91/1330-4031$02.50/0

Scheme I

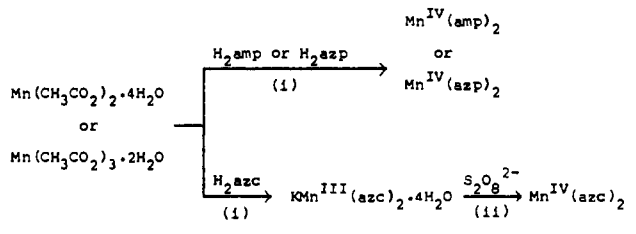

(i) air, methanol, 2 moles of KOH per mole of ligand

(ii) aqueous acetonitrile, air

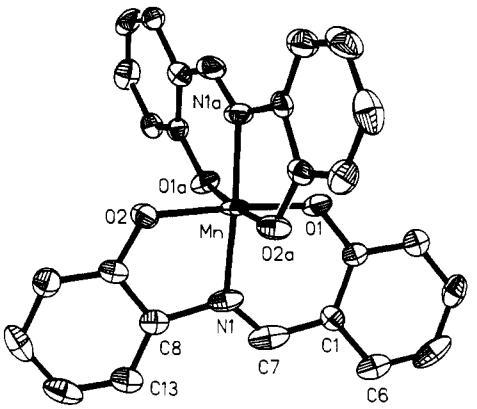

Figure 1. ORTEP plot and labeling scheme for $Mn(amp)_2$. All non-hydrogen atoms are represented by their 30% probability ellipsoids.

This work stems from our interest in the synthesis and characterization of new mononuclear manganese(IV) complexes and in the systematics of metal redox as a function of coordination environment and structure.[11,19,20] Herein we describe a group of complexes of coordination type $Mn^{IV}O_4N_2$, which exhibit a strong EPR signal near $g = 4$. The X-ray structures of two of the complexes are reported. From redox data reported in this work and elsewhere, a thermodynamic analysis of the relative efficacy of structurally authenticated alcoholic, phenolic, and carboxylic oxygen coordination (**1a–c**) on the redox potency of manga-

Mn–O(alcoholic)	Mn–O(phenolic)	Mn–O(carboxylic)
1a	**1b**	**1c**

nese(IV) has been made. The oxidizing power of the metal increases in the order **1a** < **1b** < **1c**. The implication of this on manganese binding in PS II is noted.

Results

A. Synthesis. The potentially tridentate diprotic ONO ligands (**1–3**) used in the present work are generally abbreviated as H_2L. Abbreviations of specific ligands (H_2amp, H_2azp, and H_2azc) are shown as structures **1–3**. The nitrogen function in H_2L is azo

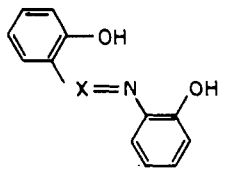

1 X=CH, H_2amp

2 X=N, H_2azp

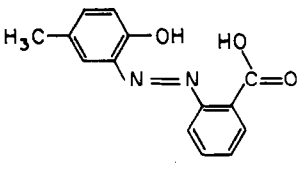

3 H_2azc

(**1**, **3**) or azomethine (**2**) and oxygen functions are phenolic (**1**, **2**) or a combination of phenolic and carboxylic (**3**).

Methods used for syntheses of the manganese complexes are summarized in Scheme I. In the presence of the diphenolic ligands (H_2amp and H_2azp), aerial oxygen rapidly oxidizes salts of bi- and trivalent manganese affording the tetravalent complex, $Mn^{IV}L_2$ in excellent yields. Under the same conditions the phenolic–carboxylic ligand H_2azc furnishes the manganese(III)

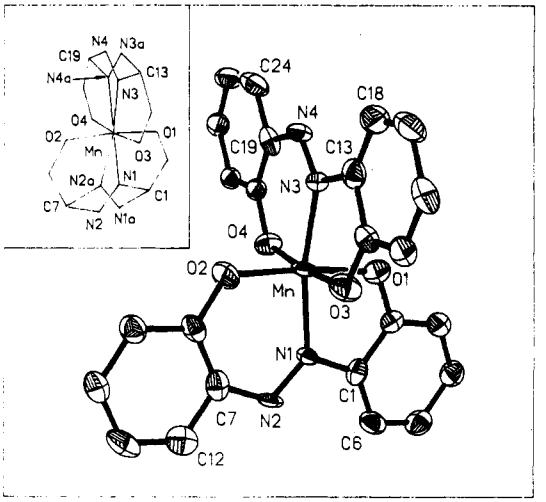

Figure 2. ORTEP plot and labeling scheme for $Mn(azp)_2$. All atoms were represented by their 30% probability ellipsoids. The disorder of the azo functions is shown in the inset.

Table I. Selected Bond Distances (Å) and Angles (deg) and Their Estimated Standard Deviations for $Mn^{IV}(amp)_2$

Distances			
Mn–O(2)	1.893 (6)	C(2)–O(1)	1.324 (9)
Mn–O(1)	1.863 (6)	C(9)–O(2)	1.346 (12)
Mn–N(1)	1.968 (8)	C(8)–N(1)	1.523 (13)
C(7)–N(1)	1.214 (12)		
Angles			
N(1)–Mn–O(1)	91.7 (3)	Mn–O(1)–C(2)	126.6 (6)
N(1)–Mn–O(2)	83.7 (3)	Mn–O(2)–C(9)	116.5 (5)
O(1)–Mn–O(1A)	87.6 (4)	Mn–N(1)–C(8)	110.5 (5)
O(2)–Mn–O(2A)	94.2 (4)	Mn–N(1)–C(7)	126.7 (9)
N(1)–Mn–O(2A)	91.1 (3)	O(1)–C(2)–C(1)	121.9 (8)
N(1)–Mn–N(1A)	172.3 (5)	O(2)–C(9)–C(8)	116.7 (8)
O(1)–Mn–O(2)	174.3 (3)	C(7)–C(1)–C(2)	124.8 (9)
O(1)–Mn–O(2A)	89.3 (3)	N(1)–C(8)–C(9)	110.6 (8)
N(1)–Mn–O(1A)	93.8 (3)	C(1)–C(7)–N(1)	124.5 (11)
O(1)–Mn–N(1A)	93.8 (3)		
O(2)–Mn–N(1A)	91.1 (3)		
O(2)–Mn–O(1A)	89.3 (3)		

Table II. Selected Bond Distances (Å) and Angles (deg) and Their Estimated Standard Deviations for $Mn^{IV}(azp)_2$

Distances			
Mn–O(4)	1.861 (4)	C(2)–O(1)	1.323 (8)
Mn–O(1)	1.873 (5)	C(8)–O(2)	1.335 (7)
Mn–O(3)	1.862 (4)	C(14)–O(3)	1.330 (7)
Mn–O(2)	1.866 (5)	C(20)–O(4)	1.321 (7)
Mn–N(3)	2.003 (10)	N(1)–N(2)	1.282 (13)
Mn–N(1)	2.011 (10)	N(3)–N(4)	1.238 (14)
C(7)–N(2)	1.408 (12)	C(13)–N(3)	1.522 (12)
C(1)–N(1)	1.445 (12)	C(19)–N(4)	1.374 (12)
Angles			
O(1)–Mn–O(2)	173.8 (2)	O(1)–Mn–O(3)	90.3 (2)
O(4)–Mn–O(2)	90.5 (2)	O(1)–Mn–N(3)	94.1 (3)
O(2)–Mn–N(3)	92.1 (3)	O(1)–Mn–N(1)	78.7 (3)
O(2)–Mn–N(1)	95.2 (3)	O(1)–Mn–O(4)	89.3 (2)
O(2)–Mn–O(3)	90.5 (2)	O(3)–Mn–O(4)	173.9 (2)
O(3)–Mn–N(1)	91.3 (3)	O(4)–Mn–N(1)	94.6 (3)
N(1)–Mn–N(3)	168.7 (4)	O(4)–Mn–N(3)	94.0 (3)
O(3)–Mn–N(3)	80.0 (3)	Mn–O(2)–C(8)	124.5 (4)
Mn–O(1)–C(2)	119.0 (4)	Mn–O(4)–C(20)	123.4 (3)
Mn–O(3)–C(14)	119.9 (4)		

(17) Kessissoglou, D. P.; Li, X.; Butler, W. M.; Pecoraro, V. L. *Inorg. Chem.* **1987**, *26*, 2487–2492.
(18) Chan, M. K.; Armstrong, W. H. *Inorg. Chem.* **1989**, *28*, 3777–3779.
(19) Chandra, S. K.; Choudhury, S. B.; Ray, D.; Chakravorty, A. *J. Chem. Soc., Chem. Commun.* **1990**, 474–475.
(20) Pal, S.; Ghosh, P.; Chakravorty, A. *Inorg. Chem.* **1985**, *24*, 3704–3706.

Table III. Magnetic Moments (298 K),[a] EPR Data (77 K),[b] and Electronic Spectral Data for MnL_2

compd	μ_{eff}, μ_B	g values[c]	UV-vis data[d] λ_{max}, nm (ϵ, M^{-1} cm^{-1})
$Mn(amp)_2$	3.82	4.20,[e] 1.82[f]	890 (1090), 640 (1945),[g] 540 (4660), 510 (4560), 385 (24 790), 365 (24 590), 320 (30 150)
$Mn(azp)_2$	4.09	4.14,[e] 1.93[f]	970 (900), 640 (3850),[g] 470 (18 600), 375 (26 300), 325 (21 300)
$Mn(azc)_2$	3.78	4.20,[e] 2.09[h]	680 (1570),[g] 540 (3875),[g] 330 (23 440), 250 (24 275)[g]

[a] In the solid state. [b] Frequency range is 9.095–9.10 GHz, and power range is 0.5–0.7 mW. [c] In dichloromethane–toluene (1:1) glass. Calculated by using DPPH as calibrant. [d] Solvent is dichloromethane. [e] Calculated at the top turnover point; the g values corresponding to base-line crossover point are, respectively, 3.35, 3.61, and 3.63. [f] Calculated at the top of the broad absorption. [g] Shoulder. [h] The signal shows six hyperfine lines with an average A of 73 G.

complex $Mn^{III}(azc)_2^-$, which is indefinitely stable in air. Oxidation to $Mn^{IV}(azc)_2$ can be done chemically by persulfate or electrochemically. The MnL_2 complexes are all nonelectrolytic and $KMn(azc)_2 \cdot 4H_2O$ acts as a 1:1 electrolyte (Λ = 118 Ω^{-1} cm^2 M^{-1}) in acetonitrile. A hydrated form of $Mn(amp)_2$ synthesized by a different route has been reported.[21] Its structural and EPR parameters are not known, and the reported metal reduction potentials do not agree with out results, vide infra.

B. Crystal and Molecular Structures. a. $Mn(amp)_2$ and $Mn(azp)_2$. The lattices of both complexes consist of discrete molecules. Perspective views and atom-labeling schemes are shown in Figures 1 and 2. Selected bond distances and angles are listed in Tables I and II. Both amp^{2-} and azp^{2-} act as tridentate meridional ONO donors. In $Mn(amp)_2$ the two ligands are equivalent (metal located on crystallographic C_2 axis). No such symmetry constraint exists for $Mn(azp)_2$. In the latter complex the molecules are packed in two different orientations. The net effect is observed as a disorder of the azo group as shown in the inset of Figure 2. Interestingly, the two orientations correspond to chemically observable isomeric forms of complexes of unsymmetrically substituted H_2azp.[22] In $Mn(amp)_2$, no parallel disorder of the azomethine function exists, but such disorder has been documented in a vanadium(V) complex of H_2amp.[23]

Due to ligand rigidity, the MnO_4N_2 coordination spheres are subject to very considerable distortions. Thus the angles at the metal center show large deviations (Tables I and II) from the ideal octahedral values of 90° and 180°. In $Mn(amp)_2$ the fragments MnO_4, $MnN_2O(1)O(2)$, and $MnN_2O(1A)O(2A)$ constitute approximate planes with a mean deviation of 0.06 Å. The interplanar angles lie in the interval 89–92°. For $Mn(azp)_2$ the corresponding parameters are 0.08 Å and 87–95°, respectively.

The Mn(amp) fragment constitutes a very mediocre plane (mean deviation 0.13 Å). The salicylaldimine (OC_7N) and the iminophenol (OC_6N) fragments are excellent individual planes (mean deviation ~0.02 Å), but there is a 15.6° fold at their intersection and this accounts for the poor overall planarity of coordinated amp^{2-}. Ligand planarity is much superior for Mn(azp) (mean deviation 0.04 Å). The fold between the two planar parts of the ligand defined in the same manner as in amp^{2-} is 4.0°. The origin of this difference between coordinated amp^{2-} and azp^{2-} is not clear but the repulsive interaction between H(7) and H(6) could be a factor favoring the augmented nonplanarity of amp^{2-}.

In $Mn(amp)_2$, the two Mn–O distances differ significantly: 1.893 (6) and 1.863 (6) Å. The shorter distance pertains to the six-membered salicylaldimine ring. In $Mn(azp)_2$ all the Mn–O distances are nearly equal, the average being 1.866 (5) Å. Azomethine nitrogen binds manganese(IV) more strongly than azo nitrogen, the Mn–N length order being $Mn(amp)_2$ < $Mn(azp)_2$.

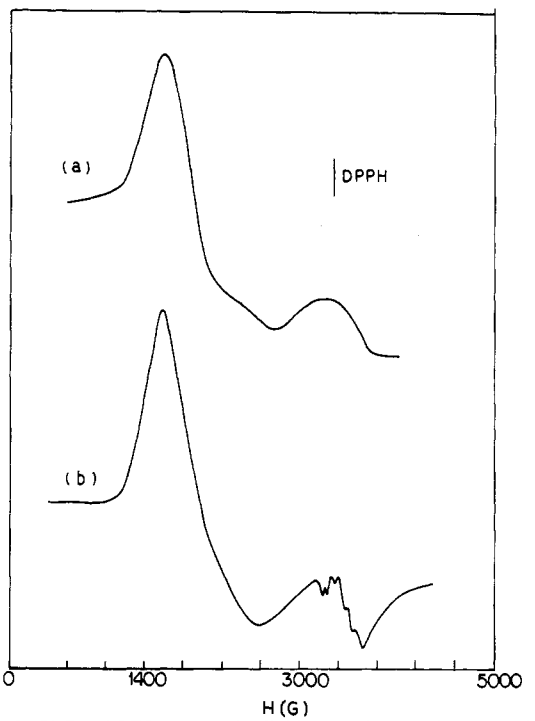

Figure 3. X-Band EPR spectra in dichloromethane–toluene (1:1) at 77 K: (a) $Mn(azp)_2$; (b) $Mn(azc)_2$.

b. Other Relevant Species. Neither $Mn(azc)_2$ nor $KMn(azc)_2 \cdot 4H_2O$ afforded X-ray quality single crystals. However their properties are entirely consistent with tridentate binding of azc^{2-} illustrated for $Mn(azc)_2$ in structure **4a**. This binding is similar

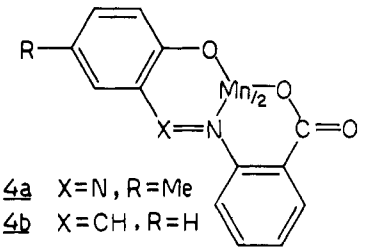

4a X=N, R=Me
4b X=CH, R=H

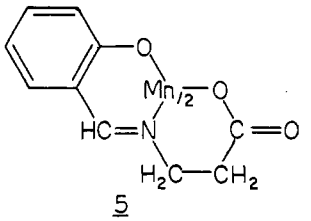

5

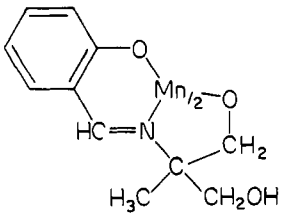

6

to that in **4b** and more importantly, in another manganese(IV) salicylaldimine complex, **5**, which has been structurally characterized.[11] The redox potentials of complex **5** (and **4b**) as well as

(21) Okawa, H.; Nakamura, M.; Kida, S. *Bull. Chem. Soc. Jpn.* **1982**, *55*, 466–470.
(22) (a) Pregosin, P. S.; Steiner, E. *Helv. Chim. Acta* **1979**, *62*, 62–66. (b) Pfitzner, H. *Angew. Chem., Int. Ed. Engl.* **1972**, *11*, 312–313. (c) Feichtmayr, F.; Pfitzner, H. *Liebigs Ann. Chem.* **1980**, 2055–2060 and references therein.
(23) Casellato, V.; Vigato, P. A.; Graziani, R.; Viladi, M.; Milani, F.; Musiani, M. M. *Inorg. Chim. Acta* **1982**, *61*, 121–128.

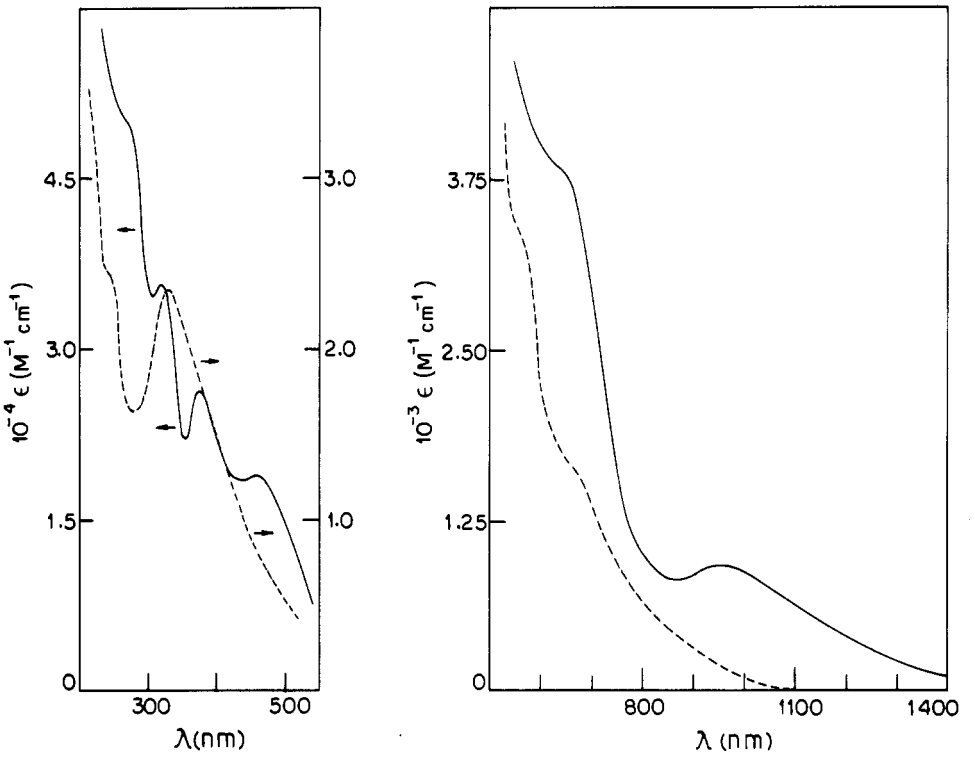

Figure 4. Electronic spectra of $Mn(azp)_2$ (—) and $Mn(azc)_2$ (---) in dichloromethane.

Table IV. Electrochemical Data[a] at 298 K

compd	solvent	Mn(IV)–Mn(III) $E°_{298}$,[b] V (ΔE_p,[c] mV)	n[d]	Mn(III)–Mn(II) $E°_{298}$,[b] V (ΔE_p,[c] mV)	ref
$Mn(amp)_2$	CH_2Cl_2	−0.03 (260)	1.02	−0.63 (300)	
	Me_2SO	−0.09 (90)		−0.95[e]	this work
$Mn(azp)_2$	CH_2Cl_2	+0.08 (160)	0.98	−0.55 (190)	
	Me_2SO	+0.15 (90)		−0.80[e]	this work
$Mn(azc)_2$	CH_2Cl_2	+0.35 (260)	1.04	−0.28 (440)	
	Me_2SO	+0.31 (70)		−0.48[e]	this work
4b	Me_2SO	+0.24 (70)		−0.60[e]	11, this work
5	Me_2SO	+0.25 (100)		−0.56[e]	11, this work
6	Me_2SO	−0.31 (200)			17

[a] Supporting electrolyte is TEAP (0.1 M); working electrode is platinum; reference electrode is SCE. [b] $E°_{298}$ is calculated as the average of anodic (E_{pa}) and cathodic (E_{pc}) peak potentials. [c] $\Delta E_p = E_{pa} - E_{pc}$. [d] Constant-potential coulometric data $n = Q/Q'$, where Q is the observed Coulomb count and Q' is the calculated could for 1e transfer. [e] Cathodic peak potential.

of **6**[17] will be considered in a later section of this paper.

C. Magnetism and Spectra. The magnetic moments of the MnL_2 complexes conform to the d^3 configuration (Table III). The pure solids do not afford well-defined EPR spectra. In frozen (77 K) 1:1 dichloromethane–toluene solution, characteristic features become observable (Figure 3, Table III). All three MnL_2 complexes show a major absorption near $g = 4$. One or more broad absorptions also occur around $g = 2$. In the case of $Mn(azc)_2$ the latter feature is sharper in nature and ^{55}Mn hyperfine structure is resolved. The manganese(III) complex $KMn(azc)_2 \cdot 4H_2O$ is EPR-silent and its magnetic moment corresponds to a high-spin d^4 configuration.

The MnL_2 complexes afford reddish brown solutions in organic solvents. A number of absorption bands are observed in the UV–vis region (Table III). Representative examples are shown in Figure 4. The diphenolato chelates $Mn(azp)_2$ and $Mn(amp)_2$ have a characteristic band near 900 nm, which is not observed in $Mn(azc)_2$.

D. Electrochemical Metal Redox. The complexes were electrochemically examined at a platinum working electrode in dimethyl sulfoxide and dichloromethane solutions. Representative cyclic voltammograms are displayed in Figure 5 and reduction potentials ($E°$ taken as equal to $E_{1/2}$) are listed in Table IV. All potentials are referenced to a saturated calomel electrode (SCE).

Two cyclic responses are observed in the potential range ±1.0 V. Constant-potential coulometry confirmed the one-electron nature of the response occurring at a more positive potential. This is assigned to the electrode reaction of eq 1. Current height

$$Mn^{IV}L_2 + e^- \rightleftharpoons Mn^{III}L_2^- \quad (1)$$

considerations support the same electron stoichiometry for the other response, which is assigned to the $Mn^{III}L_2^-$–$Mn^{II}L_2^{2-}$ couple.

In dimethyl sulfoxide solution the manganese(IV)–manganese(III) couple is quasi-reversible with a peak-to-peak separation (ΔE_p) in the range 70–90 mV (Table IV). Both the anodic and cathodic peaks of the manganese(III)–manganese(II) couple are observable in dichloromethane.[24] In dimethyl sulfoxide, the anodic peak is absent, suggesting that MnL_2^{2-} is unstable in this solvent presumably due to solvolysis.

For the diphenolato complexes, the trivalent state can be electrogenerated in solution. Thus upon exhaustive reduction of $Mn(azp)_2$ at −0.20 V in dichloromethane, one electron is consumed and the color of the solution becomes pink. This solution has the same voltammogram (initial scan anodic) as that of $Mn(azp)_2$ (initial scan cathodic). Clearly, the reduced solution contains $Mn^{III}(azp)_2^-$. Upon coulometric reoxidation of the pink solution

(24) The manganese(IV)–manganese(III) and manganese(III)–manganese(II) formal potentials of a complex described as $Mn(amp)_2 \cdot 0.5H_2O$ are reported[21] to be −0.06 and −0.76 V vs NHE, respectively, in dichloromethane. On the SCE scale the potentials work out to be −0.31 and −1.01 V. These values do not agree with our values for $Mn(amp)_2$.

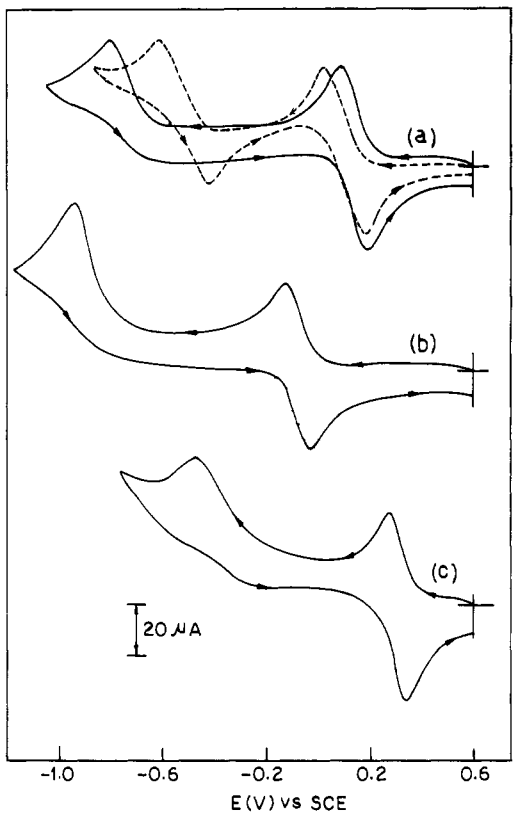

Figure 5. Cyclic voltammograms (scan rate, 50 mV s^{-1}) of $\sim 10^{-3}$ M solutions (0.1 M TEAP) of (a) $Mn(azp)_2$ in dimethyl sulfoxide (—) and in dichloromethane (- - -), (b) $Mn(amp)_2$ in dimethyl sulfoxide, and (c) $Mn(azc)_2$ in dimethyl sulfoxide at a platinum electrode (298 K).

at +0.36 V, one electrode is liberated and $Mn(azp)_2$ is re-formed quantitatively. The behavior of $Mn(amp)_2$ is analogous (reduction at −0.36 V and reoxidation at +0.30 V). The trivalent complexes $Mn(amp)_2^-$ and $Mn(azp)_2^-$ are air-sensitive. The voltammetric behavior of **4b**, **5**,[11] and **6**[17] is qualitatively similar to that of $Mn(amp)_2$, and reduction potentials in dimethyl sulfoxide are listed in Table IV.

Discussion

Mn^{IV}–N(azo) Binding. To our knowledge, the present work provides the first definitive examples of the binding of azo nitrogen to tetravalent and trivalent manganese as revealed by structure determination in the case of $Mn(azp)_2$ and by inference in the cases of $Mn(azc)_2$ and $Mn(azc)_2^-$. For the bivalent metal, one case of genuine Mn^{II}–N(azo) binding has been described recently.[25]

Oxygen Donor Variation and Reduction Potential: Implication for PS II. With this work, three structurally authenticated $Mn^{IV}O_4N_2$ complexes of meridional tridentate salicylaldimines are now available: **5**,[11] **6**,[17] and $Mn(amp)_2$. Viewed from the metal, the most significant variation among them lies in two of the oxygen donor sites successively taking the forms **1a–c**. This has provided an opportunity for scrutinizing the relative effects of alcoholato, phenolato, and carboxylato oxygen coordination on the oxidizing power of manganese(IV). The manganese(IV)–manganese(III) reduction potentials of the triad in Me_2SO (Table IV) follow the order **6** < $Mn(amp)_2$ < **5** or **1a** < **1b** < **1c**. The total shift of $E°$ between **6** and **5** is quite substantial, ~600 mV. The phenolato < carboxylato rule for $E°$ values is also obeyed by the pairs $Mn(amp)_2$ < **4b** and $Mn(azp)_2$ < $Mn(azc)_2$. This rule provides a rationale for the synthetic reactions of Scheme I: manganese(II) is oxidized by air to the tetravalent state in the presence of H_2azp but only to the trivalent state in the presence of H_2azc.

Phenolato and carboxylato oxygen functions are among the probable binders of manganese in PS II. Since water oxidation requires a high-potential oxidant (E > 1.1 V vs SCE), carboxylate binding would clearly be of advantage as far as oxygen donors are concerned. Significant evidence now exists indicating the actual existence of carboxylate binding for manganese in PS II.[1-3]

$E°_{298}$–pK Correlation. A thermodynamic scrutiny of $E°$ provides insight into the nature of the above-noted trend of formal potentials. Among similarly constituted molecules, a number of the entropy and enthalpy terms determining $E°$ remain invariant affording eq 2.[26,27] Here F is the Faraday constant, k is a constant

$$FE° = -\Delta H_f° + k \qquad (2)$$

covering the invariant quantities and $\Delta H_f°$ is the difference between the enthalpy of formation of the reduced (ML_2^-) and oxidized (ML_2) complexes taken in that order (the symbol ML_2 is being extended here to cover **5** and **6** in addition to $Mn(amp)_2$). A tetravalent complex will in general be expected to have a higher enthalpy of formation than the corresponding trivalent complex. Thus $\Delta H_f°$, defined in the sense trivalent minus tetravalent, will be generally positive (endothermic).

The variation of the Mn–O bond as in **1a–c** will cause a corresponding variation of $\Delta H_f°$ and hence $E°$. Since the Mn–O bond of types under consideration is primarily σ in character, its strength should increase as the oxygen atom becomes a better donor. Correspondingly $\Delta H_f°$ should become more positive and $E°$ more negative. The pK's of the protonated oxygen functions (alcohol, phenol, carboxylic acid) can be used as good measures of the relative σ-donor strengths of the corresponding deprotonated functions that bind the metal. The stronger the σ-donor atom is, the poorer is the acid dissociation and the higher is pK_a. Thus increase of ligand pK_a should diminish metal $E°$. This is experimentally observed. Indeed the plot of pK_a's of EtOH, PhOH and $EtCO_2H$ (15.90, 9.92, and 4.86, respectively)[28] versus the manganese(IV)–manganese(III) formal potentials of **6**, $Mn(amp)_2$, and **5** is satisfactory and linear. The probable dependence of $E°$ on pK in manganese(IV) complexes has been cursorily noted earlier.[11,17] The present work substantiates this and provides a semiquantitative basis.

An $E°$–pK correlation also applies to the nitrogen donor site. The azomethine nitrogen is a stronger donor (more basic) than the azo nitrogen as is evident in the pK's of $PhCH{=}NHPh^+$ (5.8)[29] andf $PhN{=}NHPh^+$ (2.2).[28] The formal potential order $Mn(amp)_2$ < $Mn(azp)_2$ is consistent with this.

EPR Spectra. We now briefly comment on the EPR spectra of the complexes. Pseudooctahedral d^3 species usually give rise to complex EPR spectra.[30] However, under strongly axial distortion, a simplified spectrum with two main resonances near g = 4 (strong) and g = 2 (weak) is predicted. This situation has been broadly realized in some manganese(IV) complexes,[11,14,18,19,31] and the present MnL_2 complexes also belong to this category. However, the asymmetry of the signals are good indications of the presence of low-symmetry ligand-field components. This is in qualitative agreement with the distortion of the MnO_4N_2 coordination spheres observed in crystalline $Mn(amp)_2$ and $Mn(azp)_2$. A strong g = 4 signal devoid of metal hyperfine structure

(25) (a) Basu, P.; Pal, S.; Chakravorty, A. *Inorg. Chem.* **1988**, *27*, 1848–1850. (b) Chattopadhyay, S.; Basu, P.; Pal, S.; Chakravorty, A. *J. Chem. Soc., Dalton Trans.* **1990**, 3829–3833.

(26) Mukherjee, R. N.; Rajan, O.; Chakravorty, A. *Inorg. Chem.* **1982**, *21*, 785–790.

(27) (a) Hanania, G. I. H.; Irvine, D. H.; Eaton, W. A.; George, P. *J. Phys. Chem.* **1967**, *71*, 2022. (b) Yee, E. L.; Cave, R. J.; Guyer, K. L.; Tyma, P. D.; Weaver, M. J. *J. Am. Chem. Soc.* **1979**, *101*, 1131.

(28) Perrin, D. D.; Dempsey, B.; Serjeant, E. P. *pK_a Prediction for Organic Acids and Bases*; Chapman and Hall: London and New York, 1981.

(29) Jaffe, H. H. *Chem. Rev.* **1953**, *53*, 191.

(30) (a) Pederson, E.; Toftlund, H. *Inorg. Chem.* **1974**, *13*, 1603–1612. (b) Bradley, D. C.; Copperthwaite, R. G.; Cotton, S. A.; Sales, K. D.; Gibson, J. F. *J. Chem. Soc., Dalton Trans.* **1973**, 191–194. (c) Hampel, J. C.; Morgan, L. O.; Lewis, W. B. *Inorg. Chem.* **1970**, *9*, 2064–2072.

(31) (a) Richens, D. T.; Sawyer, D. T. *J. Am. Chem. Soc.* **1979**, *101*, 3681–3683. (b) Camenzind, M. J.; Hollander, F. J.; Hill, C. L. *Inorg. Chem.* **1983**, *22*, 3776–3784.

is a characteristic feature of PS II under certain conditions. In this regard, the MnL_2 complexes are spectrally biomimetic.

Concluding Remarks

The reported complexes are bis chelates of the type $Mn^{IV}(ONO)_2$. The variation of the ONO ligands used in the present work encompasses azomethine/azo nitrogen and phenolic/carboxylic oxygen. The first example of Mn^{IV}–N(azo) binding has been structurally authenticated in $Mn(azp)_2$. The structure of its azomethine analogue $Mn(amp)_2$ is also reported. The MnO_4N_2 coordination spheres in the two complexes display large deviations from octahedral geometry. This is in qualitative agreement with the observed EPR spectra, which are characterized by a strong $g = 4$ signal. In $Mn^{IV}O_4N_2$ complexes reported here and elsewhere, variation of two of the four oxygen donor functions increases the oxidizing power of manganese(IV) in the order alcoholic < phenolic < carboxylic (**6** < $Mn(amp)_2$ < **5**). The formal potentials of the manganese(IV)–manganese(III) couple increase by a remarkable ~600 mV between **6** and **5**. The thermodynamic basis of the variation has been analyzed and a correlation between the pK of the potential oxygen function and the manganese(IV)–manganese(III) reduction potential established. The probable significance of the results with respect to Mn–O(carboxylate) binding in PS II is noted.

Experimental Section

Materials. $Mn(OAc)_3 \cdot 2H_2O$ was prepared as reported.[32] Electrochemically pure dichloromethane, acetonitrile, and tetraethylammonium perchlorate (TEAP) were obtained as before.[33] All other chemicals and solvents were of analytical grade and used as obtained.

Physical Measurements. Electronic spectra were recorded with an Hitachi 330 spectrophotometer. X-Band EPR spectra were collected on a Varian E-109C spectrometer fitted with a quartz Dewar flask for low-temperature measurements (liquid nitrogen, 77 K). DPPH (g = 2.0037) was used to calibrate the EPR spectra. Electrochemical measurements were performed on a PAR Model 370-4 electrochemistry system as reported earlier.[11] All potentials reported in this work are uncorrected for junction contribution. Magnetic susceptibilities were measured by using a PAR-155 vibrating sample magnetometer fitted with a Walker Scientific L 75FBAL magnet. Solution (~10^{-3} M) electrical conductivities were measured with the help of a Philips PR 9500 bridge. A Perkin-Elmer 240C elemental analyzer was used to collect microanalytical data (C, H, N).

Preparation of Compounds. The ligands *N*-(2-hydroxyphenyl)salicylaldimine (H_2amp), 2,2′-dihydroxyazobenzene (H_2azp) and 2-hydroxy-2′-carboxy-5-methylazobenzene (H_2azc) were prepared by reported procedures.[34,35] $Mn(amp)_2$, $Mn(azp)_2$, and $KMn(azc)_2 \cdot 4H_2O$ can be prepared either from $Mn(OAc)_2 \cdot 4H_2O$ or $Mn(OAc)_3 \cdot 2H_2O$. Preparative procedure from the latter is described below.

Bis(*N*-(2-hydroxyphenyl)salicylaldiminato)manganese(IV), Mn(amp)$_2$. To a methanolic solution (20 mL) of H_2amp (0.2 g, 0.94 mmol) was added 0.10 g (1.78 mmol) of KOH. On addition of 0.125 g (0.47 mmol) of $Mn(OAc)_3 \cdot 2H_2O$ to this solution, the red color changed to brown. The mixture was stirred at room temperature in air for 6 h. A dark solid separated, which was filtered, washed thoroughly with methanol and a little water, and finally dried in vacuo over P_4O_{10}. Yield: 0.20 g (90%). Anal. Calcd for $MnC_{26}H_{18}N_2O_4$: Mn, 11.52; C, 65.42; H, 3.77; N, 5.87. Found: Mn, 11.24; C, 65.16; H, 3.70; N, 5.79.

Bis(2,2′-dihydroxyazobenzenato)manganese(IV), Mn(azp)$_2$. To a methanolic solution (20 mL) of H_2azp (0.20 g, 0.93 mmol) was added KOH (0.10 g, 1.78 mmol). Addition of $Mn(OAc)_3 \cdot 2H_2O$ (0.125 g, 0.47 mmol) to the solution followed by stirring in air for 0.5 h afforded a brown solution, which upon evaporation to dryness yield a solid, which was crystallized from a dichloromethane–hexane (1:1) solvent mixture. Yield: 0.15 g (67%). Anal. Calcd for $MnC_{24}H_{16}N_4O_4$: Mn, 11.47; C, 60.13; H, 3.34; N, 11.69. Found: Mn, 11.32; C, 61.05; H, 3.29; N, 11.61.

Potassium Bis(2-hydroxy-2′-carboxy-5-methylazobenzenato)manganate(III) Tetrahydrate, $KMn(azc)_2 \cdot 4H_2O$. To a methanolic solution (30 mL) of H_2azc (0.40 g, 1.56 mmol) was added 0.175 g (3.13 mmol) of KOH. When $Mn(OAc)_3 \cdot 2H_2O$ (0.2 g, 0.75 mmol) was added, the color of the solution changed from red to violet. The volume of the solution was reduced by stirring in air at room temperature till a solid precipitated. It was collected by filtration and washed with ether followed by water and dried in vacuo over P_4O_{10}. Yield: 0.27 g (60%). Anal. Calcd for $KMnC_{28}H_{28}N_4O_{10}$: Mn, 8.15; C, 49.85; H, 4.15; N, 8.31. Found: Mn, 8.04; C, 49.22; H, 4.21; N, 7.86. μ_{eff} = 4.94 μ_B. UV–vis spectral data in acetonitrile (λ_{max}, nm (ϵ, M^{-1} cm^{-1})): 1150 (200), 470 (8800), 325 (27150), 250 (33900, sh).

Bis(2-hydroxy-2′-carboxy-5-methylazobenzenato)manganese(IV), Mn(azc)$_2$. Chemical Synthesis. An aqueous solution (25 mL) of $K_2S_2O_8$ (0.20 g, 0.74 mmol) was added to a solution of $KMn(azc)_2 \cdot 4H_2O$ (0.56 g, 0.83 mmol) in 15 mL of acetonitrile. The mixture was stirred at room temperature for 15 min. The color of the solution changed from violet to brown. It was then was extracted with dichloromethane. Reduction of the volume of the dichloromethane extract followed by addition of hexane yielded a solid product. This was collected by filtration and dried under vacuo. Yield: 0.30 g (64%).

Electrosynthesis. A solution of 100 mg (0.15 mmol) of $KMn(azc)_2 \cdot 4H_2O$ in 30 mL of dry acetonitrile (0.1 M NH_4PF_6) was oxidized coulometrically at a constant potential of 0.62 V vs SCE in nitrogen atmosphere. As the oxidation proceeded, the color of the solution changed from violet to brown. The solution was evaporated to dryness after complete oxidation, the resultant solid was extracted with dichloromethane, and the extract, upon evaporation to dryness, afforded $Mn(azc)_2$. Yield: 70 mg (85%). Anal. Calcd for $MnC_{28}H_{20}N_4O_6$: Mn, 9.76; C, 59.69; H, 3.55; N, 9.95. Found: Mn, 9.52; C, 59.19; H, 3.47; N, 9.87.

X-ray Structure Determination. Dark parallelepiped single crystals of $Mn(amp)_2$ and $Mn(azp)_2$ were grown (298 K) by slow diffusion of hexane into dichloromethane solution. Data collection was performed

Table V. Crystallographic Data for $Mn(amp)_2$ and $Mn(azp)_2$

	$Mn(amp)_2$	$Mn(azp)_2$
chem formula	$C_{26}H_{18}O_4N_2Mn$	$C_{24}H_{16}O_4N_4Mn$
fw	477.4	479.3
space group	$C2/c$	$P\bar{1}$
a, Å	20.163 (12)	7.766 (5)
b, Å	7.921 (4)	10.377 (5)
c, Å	12.994 (10)	12.964 (5)
α, deg		92.80 (3)
β, deg	97.65 (5)	90.33 (5)
γ, deg		102.92 (4)
V, Å^3	2057 (2)	1016.8 (9)
Z	4	2
T, °C	23	23
λ	0.71073	0.71073
ρ_{calcd}, g cm^{-3}	1.542	1.566
μ, cm^{-1}	6.52	6.62
transm coeff	0.8625–0.9151	0.8010–0.9430
R^a	7.05	7.02
R_w^b	5.92	8.00

$^a R = \sum||F_o| - |F_c||/\sum|F_o|$. $^b R_w = [\sum w(|F_o| - |F_c|)^2/\sum w|F_o|^2]^{1/2}$; $w^{-1} = \sigma^2(|F_o| + g|F_o|^2)$; g = 0.0001 for $Mn(amp)_2$ and 0.001 for $Mn(azp)_2$.

Table VI. Atomic Coordinates (×10^4) and Equivalent^a Isotropic Displacement Coefficients (Å^2 × 10^3) for $Mn(amp)_2$

	x	y	z	U(eq)
Mn	0	3544 (3)	2500	40 (1)
O(1)	560 (3)	1846 (8)	3109 (4)	53 (3)
O(2)	−638 (3)	5169 (8)	1947 (4)	52 (3)
N(1)	−466 (5)	3710 (11)	3734 (6)	55 (3)
C(1)	294 (5)	2143 (12)	4842 (7)	42 (3)
C(2)	694 (5)	1509 (13)	4114 (6)	41 (3)
C(3)	1207 (5)	416 (13)	4450 (7)	50 (4)
C(4)	1345 (6)	−1 (13)	5471 (8)	63 (4)
C(5)	950 (9)	597 (17)	6171 (8)	80 (6)
C(6)	438 (6)	1640 (15)	5889 (7)	57 (4)
C(7)	−272 (6)	3170 (13)	4596 (8)	67 (5)
C(8)	−1114 (5)	4705 (12)	3484 (7)	45 (4)
C(9)	−1162 (5)	5416 (12)	2471 (7)	43 (3)
C(10)	−1701 (6)	6363 (14)	2116 (7)	57 (4)
C(11)	−2206 (5)	6688 (15)	2732 (9)	71 (5)
C(12)	−2128 (7)	5975 (16)	3740 (9)	77 (5)
C(13)	−1600 (6)	5034 (14)	4088 (7)	60 (4)

^{a} Equivalent isotropic U defined as one-third of the trace of the orthogonalized U_{ij} tensor.

(32) Brauer, G., Ed. *Handbook of Preparative Inorganic Chemistry*: Academic Press: New York, 1965; Vol. 2, pp 1469–1470.
(33) Datta, D.; Mascharak, P. K.; Chakravorty, A. *Inorg. Chem.* **1981**, *20*, 1673–1679.
(34) Drew, H. D. K.; Laudguist, J. K. *J. Chem. Soc.* **1938**, 292–304.
(35) Alyea, E. A.; Malek, A. *Can. J. Chem.* **1975**, *53*, 939.

Table VII. Atomic Coordinates ($\times 10^4$) and Equivalent[a] Isotropic Displacement Coefficients ($Å^2 \times 10^3$) for $Mn(azp)_2$

	x	y	z	U(eq)
Mn	1497 (1)	8684 (1)	7198 (1)	42 (1)
O(1)	2094 (6)	7344 (4)	6347 (3)	62 (2)
O(2)	981 (6)	10140 (4)	7931 (4)	70 (2)
O(3)	-865 (6)	8106 (4)	6789 (3)	66 (2)
O(4)	3807 (5)	9129 (4)	7713 (3)	57 (2)
N(1)	2077 (11)	9614 (8)	5876 (8)	38 (3)
N(3)	613 (14)	7480 (10)	8335 (7)	37 (3)
N(2)	1968 (11)	10782 (8)	5648 (8)	44 (3)
N(4)	1323 (15)	7253 (9)	9143 (7)	53 (4)
N(3A)	69 (19)	6878 (12)	8882 (12)	28 (4)
N(1A)	2312 (22)	10139 (22)	5300 (14)	44 (6)
N(2A)	1774 (20)	10167 (19)	6237 (11)	34 (5)
N(4A)	1477 (22)	7713 (18)	8514 (16)	29 (5)
C(1)	2694 (7)	8881 (6)	5035 (5)	51 (2)
C(2)	2657 (7)	7618 (6)	5394 (4)	48 (2)
C(3)	3211 (8)	6715 (6)	4751 (5)	58 (2)
C(4)	3780 (9)	7016 (7)	3774 (5)	63 (3)
C(5)	3787 (9)	8283 (8)	3414 (5)	67 (3)
C(6)	3260 (8)	9185 (6)	4030 (5)	60 (2)
C(7)	1409 (8)	11520 (7)	6469 (5)	57 (2)
C(8)	950 (7)	11281 (6)	7527 (5)	51 (2)
C(9)	509 (8)	12287 (6)	8137 (5)	59 (2)
C(10)	474 (9)	13497 (6)	7717 (6)	62 (3)
C(11)	873 (9)	13713 (7)	6679 (7)	72 (3)
C(12)	1336 (9)	12746 (8)	6083 (6)	68 (3)
C(13)	-1324 (9)	6768 (6)	8236 (5)	56 (2)
C(14)	-1951 (8)	7224 (5)	7333 (5)	48 (2)
C(15)	-3699 (8)	6773 (6)	7030 (5)	53 (2)
C(16)	-4820 (9)	5911 (6)	7627 (6)	64 (3)
C(17)	-4190 (12)	5467 (7)	8532 (6)	73 (3)
C(18)	-2495 (13)	5888 (7)	8824 (5)	73 (3)
C(19)	3073 (8)	7892 (6)	9233 (5)	53 (2)
C(20)	4290 (8)	8737 (5)	8603 (4)	43 (2)
C(21)	6043 (8)	9155 (5)	8946 (4)	45 (2)
C(22)	6536 (8)	8763 (6)	9883 (5)	55 (2)
C(23)	5332 (11)	7972 (7)	10500 (5)	68 (3)
C(24)	3657 (12)	7535 (7)	10178 (6)	73 (3)

[a] Equivalent isotropic U defined as one-third of the trace of the orthogonalized U_{ij} tensor.

on a Nicolet R3m/V automated diffractometer using graphite monochromated Mo Kα radiation (λ = 0.710 73 Å). Significant crystal data and data collection parameters are listed in Table V. The unit cell parameters of $Mn(amp)_2$ were determined by a least-squares fit of 22 reflections selected from a rotation photograph (2θ ranges 5–20°). For $Mn(azp)_2$, 21 reflections selected by a random search routine (2θ ranges 11–28°) were used. Lattice dimensions and Laue groups were checked by axial photography. Systematic absences led to the identification of the space group as Cc or $C2/c$ for $Mn(amp)_2$. The structure was successfully solved in the latter space group. In contrast $Mn(azp)_2$ is triclinic, $P\bar{1}$.

During data collection, the parameters were kept fixed as follows for both complexes: ω-ranges of 1.8°; variable scan speed between 3.0 and 30.0 min^{-1}; ratio of background/scan time 0.5. Two check reflections were measured after every 98 reflections during data collection to monitor crystal stability. No significant intensity reduction was observed in the 22 h ($Mn(amp)_2$) and 88 h ($Mn(azp)_2$) of exposure to X-rays. Absorption correction was done numerically for $Mn(amp)_2$; for $Mn(azp)_2$, it was done emperically on the basis of azimuthal scans[36] of six reflections.

All calculations for data reduction, structure solution, and refinement were done on a MicroVAX II computer with the programs of SHELXTL-PLUS.[37] The metal position of $Mn(amp)_2$ was located from a Patterson map, and the remainder of the non-hydrogen atoms emerged from a difference Fourier map. For $Mn(azp)_2$ the structure was solved by direct methods. In both cases, the structures were refined by full-matrix least-squares procedures. All non-hydrogen atoms were refined anisotropically. Hydrogen atoms were included in calculated positions with fixed isotropic thermal parameters. The highest difference Fourier peaks were 0.34 and 0.70 e/Å^3 for $Mn(amp)_2$ and $Mn(azp)_2$, respectively. Atomic coordinates and isotropic thermal parameters for both structures are collected in Tables VI and VII.

Acknowledgment. Crystallography was performed at the National Single Crystal Diffractometer Facility at the Department of Inorganic Chemistry, Indian Association for the Cultivation of Science. Financial support received from the Department of Science and Technology, New Delhi, and Council of Scientific and Industrial Research, New Delhi, are acknowledged.

Supplementary Material Available: Listings of anisotropic thermal parameters (Tables VIII and IX), complete bond distances (Tables X and XI) and angles (Tables XII and XIII), hydrogen atom positional parameters (Tables XIV and XV), and structure determination summaries (Tables XVI and XVII) for $Mn(amp)_2$ and $Mn(azp)_2$ (13 pages); listings of observed and calculated structure factors for the above two complexes (14 pages). Ordering information is given on any current masthead page.

(36) North, A. C. T.; Philips, D. C.; Mathews, F. S. *Acta Crystallogr., Sect. A* **1968**, *24*, 351–359.
(37) Sheldrick, G. M. *SHELXTL-PLUS 88, Structure Determination Software Programs*; Nicolet Instrument Corp.: Madison, WI, 1988.